

Dynamic nuclear polarization enhanced magnetic field sensitivity and decoherence spectroscopy of an ensemble of near-surface nitrogen-vacancy centers in diamond

Kento Sasaki, Ed E. Kleinsasser, Zhouyang Zhu, Wen-Di Li, Hideyuki Watanabe, Kai-Mei C. Fu, Kohei M. Itoh, and Eisuke Abe

Citation: [Appl. Phys. Lett.](#) **110**, 192407 (2017); doi: 10.1063/1.4983350

View online: <http://dx.doi.org/10.1063/1.4983350>

View Table of Contents: <http://aip.scitation.org/toc/apl/110/19>

Published by the [American Institute of Physics](#)

Articles you may be interested in

High reverse breakdown voltage Schottky rectifiers without edge termination on Ga₂O₃
Applied Physics Letters **110**, 192101 (2017); 10.1063/1.4983203

Room-temperature five-tesla coercivity of a rare-earth-free shell-ferromagnet
Applied Physics Letters **110**, 192406 (2017); 10.1063/1.4983199

Investigation of spin scattering mechanism in silicon channels of Fe/MgO/Si lateral spin valves
Applied Physics Letters **110**, 192401 (2017); 10.1063/1.4982966

Cold exciton electroluminescence from air-suspended carbon nanotube split-gate devices
Applied Physics Letters **110**, 191101 (2017); 10.1063/1.4983278

Strong perpendicular magnetic anisotropy energy density at Fe alloy/HfO₂ interfaces
Applied Physics Letters **110**, 192403 (2017); 10.1063/1.4983170

Nuclear quantum-assisted magnetometer
Review of Scientific Instruments **88**, 013702 (2017); 10.1063/1.4973449



Dynamic nuclear polarization enhanced magnetic field sensitivity and decoherence spectroscopy of an ensemble of near-surface nitrogen-vacancy centers in diamond

Kento Sasaki,¹ Ed E. Kleinsasser,² Zhouyang Zhu,^{3,4} Wen-Di Li,^{3,4} Hideyuki Watanabe,⁵ Kai-Mei C. Fu,^{2,6} Kohei M. Itoh,^{1,7,a)} and Eisuke Abe^{7,b)}

¹School of Fundamental Science and Technology, Keio University, 3-14-1 Hiyoshi, Kohoku-ku, Yokohama 223-8522, Japan

²Department of Electrical Engineering, University of Washington, Seattle, Washington 98195-2500, USA

³HKU-Shenzhen Institute of Research and Innovation (HKU-SIRI), Shenzhen 518000, China

⁴Department of Mechanical Engineering, The University of Hong Kong, Pokfulam, Hong Kong, China

⁵Correlated Electronics Group, Electronics and Photonics Research Institute, National Institute of Advanced Industrial Science and Technology (AIST), Tsukuba Central 5, 1-1-1 Higashi, Tsukuba, Ibaraki 305-8565, Japan

⁶Department of Physics, University of Washington, Seattle, Washington 98195-1560, USA

⁷Spintronics Research Center, Keio University, 3-14-1 Hiyoshi, Kohoku-ku, Yokohama 223-8522, Japan

(Received 24 November 2016; accepted 26 April 2017; published online 9 May 2017)

We perform pulsed optically detected electron spin resonance to measure the DC magnetic field sensitivity and electronic spin coherence time T_2 of an ensemble of near-surface, high-density nitrogen-vacancy centers engineered to have a narrow magnetic resonance linewidth. Combining pulsed spectroscopy with dynamic nuclear polarization, we obtain the photon-shot-noise-limited DC magnetic sensitivity of $35 \text{ nT Hz}^{-0.5}$. We find that T_2 is controlled by instantaneous diffusion, enabling decoherence spectroscopy on residual nitrogen impurity spins in the diamond lattice and a quantitative determination of their density. The demonstrated high DC magnetic sensitivity and decoherence spectroscopy are expected to broaden the application range for two-dimensional magnetic imaging. Published by AIP Publishing. [<http://dx.doi.org/10.1063/1.4983350>]

Submicron scale, two-dimensional (2D) magnetic imaging has potential applications in biological and physical sciences.^{1,2} The realization of utilizing an ensemble of nitrogen-vacancy (NV) centers in diamond is particularly attractive due to its high magnetic sensitivity at ambient conditions.^{3–10} When NV-based sensing is carried out with continuous wave (CW) optically detected magnetic resonance (ODMR), the photon-shot-noise-limited DC magnetic field sensitivity η_{sn} is estimated as

$$\eta_{\text{sn}}^{(\text{cw})} = \frac{h}{g\mu_B} \frac{\delta\nu}{C\sqrt{I_0}}, \quad (1)$$

where $h/g\mu_B = 36 \text{ }\mu\text{T/MHz}$ is the inverse of the gyromagnetic ratio of the NV electronic spins, I_0 is the count rate of photons from the NV centers in a unit area ($1 \text{ }\mu\text{m}^2$) under the off-resonance condition, $\delta\nu$ is the ODMR linewidth, and C is the ODMR contrast (the ratio of the photon counts on and off resonances).^{11,12} Equation (1) suggests that simultaneously achieving a high NV density and a narrow linewidth is desired to improve $\eta_{\text{sn}}^{(\text{cw})}$. In addition, the NV sensor must be located as close as possible to a magnetic specimen; it is crucial to have an NV ensemble near the diamond surface.^{13,14}

Recently, some of the present authors have reported the successful creation of a 100-nm-thick layer of NV ensembles at a diamond surface with a density of 10^{17} cm^{-3} and a $\delta\nu$ of $\sim 200 \text{ kHz}$.¹⁵ This was achieved by a combination of

chemical vapor deposition (CVD) growth of a nitrogen-doped, nuclear-spin-free ^{12}C (99.9%) diamond film¹⁶ and subsequent helium ion implantation to introduce vacancies into the film. The detailed procedure for the NV formation and the characterization of the NV ensemble by photoluminescence (PL) spectroscopy and CW ODMR are given in Ref. 15.

In this paper, we show that, by concurrently applying pulsed ODMR and dynamic nuclear polarization (DNP) techniques to the same diamond sample, it is possible to realize an η_{sn} of $35 \text{ nT Hz}^{-0.5}$. We also examine the coherence properties of the NV ensemble to extract quantitative information on residual paramagnetic impurities in the sample. This is an example of “decoherence spectroscopy/imaging,” in which magnetic signals are detected via the change in spin coherence time T_2 .^{17–23} This method is applicable to identify magnetic signals external to the sample, providing another tool for ensemble-based 2D magnetic field imaging.

We first recap the main result of Ref. 15 by performing CW ODMR at an external magnetic field B_0 of 1.5 mT . The squares (\square) in Fig. 1 are the measured $\delta\nu$ (top) and C (middle) together with $\eta_{\text{sn}}^{(\text{cw})}$ estimated from Eq. (1) (bottom) as functions of the microwave power P_{mw} , demonstrating the minimum sensitivity of $124 \text{ nT Hz}^{-0.5}$. The measurement setup in the present work is a home-built confocal microscope combined with microwave circuitry, enabling CW and pulsed ODMR of single and ensemble NV centers. Throughout this work, B_0 is applied parallel to one of four NV axes, and the $m_S = 0 \leftrightarrow -1$ transition of the NV ensemble aligned to the field is examined, unless otherwise

^{a)}Electronic mail: kitoh@appi.keio.ac.jp

^{b)}Electronic mail: e-abe@keio.jp

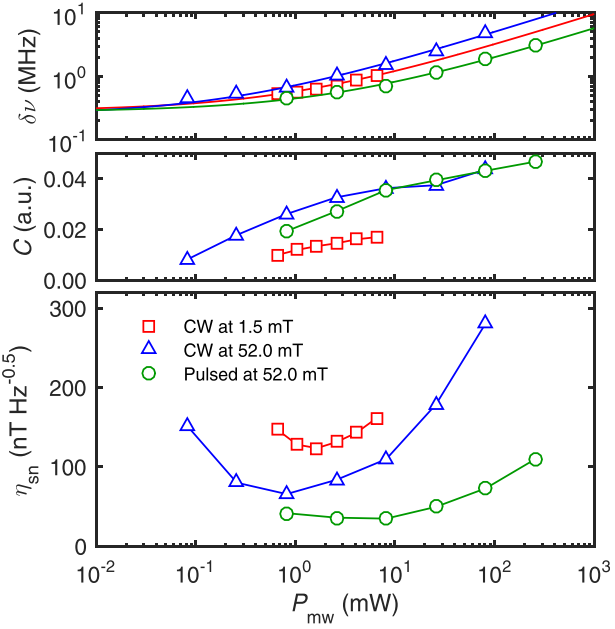


FIG. 1. $\delta\nu$ (top), C (middle), and η_{sn} (bottom) as functions of P_{mw} measured at the input port of the PCB board on which the sample is mounted. The solid lines in the top panel are fits to $\delta\nu_a + bP_{\text{mw}}^{0.5}$. The laser power P_L was optimized at $100 \mu\text{W}$ and 1.4mW for CW and pulsed experiments, respectively. The full-width-at-half-maximum of the laser spot was 520nm , corresponding to ~ 2100 NV centers in the focal volume. The optimized sensitivity $\eta_{\text{sn}}^{(\text{pulsed})} = 35 \text{nT Hz}^{-0.5}$ was obtained at P_{mw} of 8.2mW , with $\delta\nu = 718 \text{kHz}$ and $C = 0.036$.

mentioned. The relative improvement in $\eta_{\text{sn}}^{(\text{cw})}$ over the previous result ($170 \text{nT Hz}^{-0.5}$ in Ref. 15) is attributed to the differences in collection efficiency and measurement location within the sample.

As is evident from Eq. (1), the magnetic sensitivity can be improved by optimizing $\delta\nu$, C , and I_0 . Indeed, the low-field data in Fig. 1 show an interplay between $\delta\nu$ and C ; the narrowing of $\delta\nu$ as decreasing P_{mw} is countered by the reduction of C , and $\eta_{\text{sn}}^{(\text{cw})}$ takes its minimum at an intermediate value of $P_{\text{mw}} = 1.64 \text{mW}$. We observe $\delta\nu = \delta\nu_a + bP_{\text{mw}}^{0.5}$ with $\delta\nu_a \approx 250 \text{kHz}$ [solid line in the top panel of Fig. 1]. On the other hand, as demonstrated for a single NV center,²⁴ C and I_0 can be further improved, respectively, by employing the DNP of ^{14}N nuclei ($I=1$) associated with the NV centers and pulsed ODMR.

It is well-established that the excited state of the NV center experiences a level anticrossing near 50mT . In this condition, the optical pumping of the NV electronic spins polarizes the ^{14}N nuclei into the $m_I=1$ state owing to electron-nuclear flip-flops.^{25,26} Figure 2(a) plots CW ODMR spectra taken at 1.5mT and 52.0mT , demonstrating clear DNP in the latter. We then repeat the measurements at 52.0mT [\triangle in Fig. 1] to obtain the minimum sensitivity of $66 \text{nT Hz}^{-0.5}$ at $P_{\text{mw}} = 0.82 \text{mW}$.

In the DNP condition, by pumping the three nuclear spin states into a single state, we should ideally achieve a factor-of-three enhancement of C and thus $\eta_{\text{sn}}^{(\text{cw})}$. However, at a given P_{mw} , C under the DNP is typically only twice as deep as that at low fields. Also, the values of C giving the minimum sensitivities are 1.5% at 1.5mT and 2.6% at 52.0mT [Fig. 2(a)], which are reflected in the obtained sensitivities ($124 \text{nT Hz}^{-0.5}$ vs. $66 \text{nT Hz}^{-0.5}$). C is determined by a

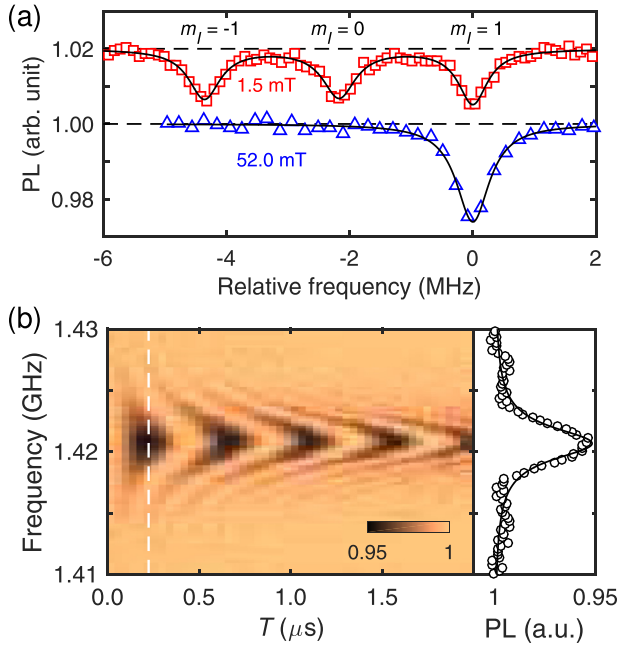


FIG. 2. (a) CW ODMR spectra at $B_0 = 1.5 \text{mT}$ and $P_{\text{mw}} = 1.64 \text{mW}$ (shifted upward by 0.02 for clarity) and at $B_0 = 52.0 \text{mT}$ and $P_{\text{mw}} = 0.82 \text{mW}$. (b) An example of pulsed spectroscopy. The cross section at $T_\pi = 222 \text{ns}$ is fitted by a Lorentzian.

complicated interplay between T_1 , T_2^* , and other optical transition probabilities between the NV electronic energy levels (e.g., Eq. (A5) of Ref. 24). We have examined several physical parameters of our NV ensemble to reproduce the observed C but have not reached a satisfactory explanation. We leave a detailed analysis on this as a future work.

In CW ODMR at a fixed P_{mw} , increasing optical excitation power simultaneously increases I_0 and $\delta\nu$ while decreasing C .²⁴ This leads to an optimal optical power well below the saturation intensity of the NV center. On the other hand, pulsed ODMR temporally separates the optical pumping from the spin manipulation. A higher laser power can be used to significantly increase I_0 while keeping C and $\delta\nu$ intact.²⁴ An example of pulsed spectroscopy, C as a function of the microwave burst time (T) and the microwave frequency, is shown in Fig. 2(b). We denote the experimental sequence as $\tau_I - T - \tau_R$, where $\tau_{I,R}$ are the durations of green laser excitation for spin initialization and readout. By varying the microwave frequency around the $m_I=1$ resonance, a chevron pattern typical of pulsed spectroscopy is observed. The cross section at the π pulse condition ($T_\pi = 222 \text{ns}$) is also shown in Fig. 2(b), from which we deduce $\delta\nu$ and C [\circ in Fig. 1]. η_{sn} for pulsed ODMR is given by^{15,24}

$$\eta_{\text{sn}}^{(\text{pulsed})} = \frac{\hbar}{g\mu_B} \frac{\delta\nu}{C} \sqrt{\frac{(\pi\delta\nu)^{-1} + \tau_I + \tau_R}{\tau_R I_0}}, \quad (2)$$

and we obtain the minimum sensitivity of $35 \text{nT Hz}^{-0.5}$ for our system.

Through time-resolved fluorescence measurements (data not shown), we optimized τ_I and τ_R as $4.5 \mu\text{s}$ and $1.5 \mu\text{s}$, respectively. These spin initialization and readout times, several times longer than the case of a single NV center

(typically about 1 μ s and a few 100 ns, respectively), currently limit the achievable $\eta_{\text{sn}}^{(\text{pulsed})}$. The long $\tau_{\text{I},\text{R}}$ are attributed to the Gaussian profile of the laser spot. Calculations suggest that 58% of the total fluorescence intensity arise from the region outside of the FWHM of the profile, and the NV ensemble existing in this region is subject to substantially lower laser power, resulting in insufficient initialization for shorter τ_{I} . A long initialization time due to the laser spot profile has also been discussed in Ref. 27.

Having demonstrated the potential of this sample for 2D DC magnetic sensing, we next measure T_2 using a Hahn echo sequence ($\tau_{\text{I}} - T_{\pi/2} - \tau - T_\pi - \tau - T_{\pi/2} - \tau_{\text{R}}$) and carry out ensemble-based decoherence spectroscopy. Figure 3(a) shows three representative Hahn echo decay curves at around 50 mT, all described well by single-exponential decays. We define T_2 by fitting the echo decay curves as $A \exp(-2\tau/T_2)$. A detailed B_0 -dependence of the decoherence rate shown in Fig. 3(c) reveals a multi-peak structure. As depicted in Fig. 3(b), the peak positions [listed in Table I] coincide with the simultaneous spin resonances (SSRs) of the NV and P1 centers: $S = \frac{1}{2}$ substitutional nitrogen impurities with C_{3v} symmetry.^{28,29} In a dipolarly coupled electron spin system, the refocusing pulse flips resonant spins within its bandwidth, instantly changing local dipolar magnetic fields experienced by the individual NV electronic spins: a process known as the instantaneous diffusion (ID). At the SSR, the NV decoherence is accelerated by

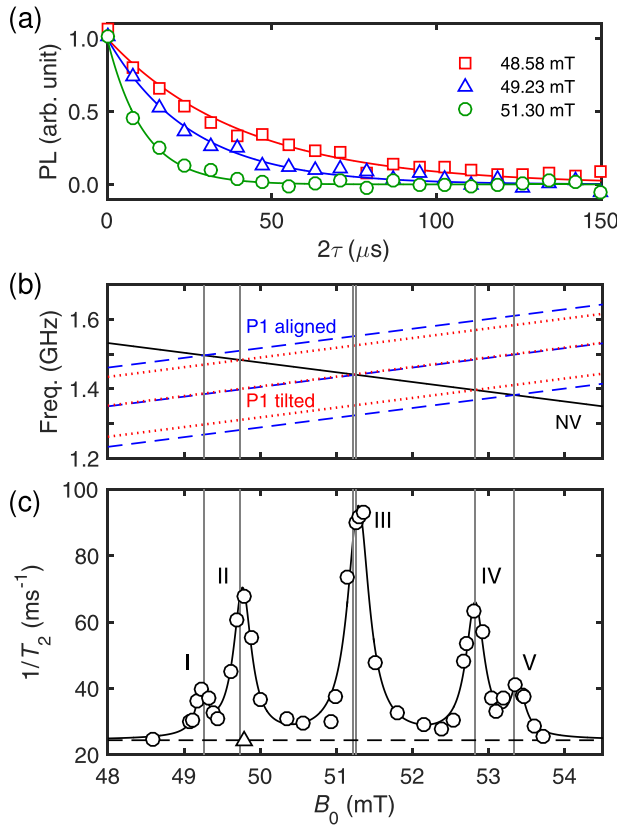


FIG. 3. (a) Hahn echo decays of the NV ensemble at around $B_0 = 50$ mT. The solid lines are fits by single-exponential decays. (b) The transition frequencies of the NV centers (solid line, $m_s = 0 \leftrightarrow -1$ with $m_l = 1$) and the P1 centers aligned with B_0 (dashed lines) and tilted from B_0 (dotted lines). The unit and scale of the horizontal axis are the same as (c). The vertical lines indicate B_0 at which the SSRs occur. (c) T_2^{-1} as a function of B_0 .

TABLE I. Analysis of Fig. 3(c). The peak positions are determined by a quintuple-Lorentzian fit. $(T_{\text{id}}^{(i)})^{-1}$ specifies $(T_{\text{id}})^{-1}$ at the i th peak after subtraction of $(T_2^{\text{base}})^{-1}$. N_i is the impurity density.

Peak	B_0 (mT)	$(T_{\text{id}}^{(i)})^{-1}$ (ms^{-1})	$N_i (10^{17} \text{ cm}^{-3})$
I	49.23	12.6	0.19
II	49.77	44.8	0.68
III	51.29	70.0	1.05
IV	52.82	40.2	0.61
V	53.38	14.8	0.22

the increased number of flipped spins. In the case of a homogeneous electron-spin distribution, the ID decay has a form of single-exponential $\exp(-2\tau/T_{\text{id}})$ with T_{id} given by^{30,31}

$$\frac{1}{T_{\text{id}}} = DN \sin^2\left(\frac{\beta}{2}\right), \quad \text{with } D = \frac{\pi \mu_0 g^2 \mu_B^2}{9\sqrt{3} \hbar}. \quad (3)$$

Here, μ_0 is the vacuum permeability, N is the density of spins rotated, and β is the flip angle of the refocusing pulse. We are thus able to extract the densities of the P1 spins from the increased decoherence rate at the respective peaks.

To do so, we first define the *baseline* decoherence rate $(T_2^{\text{base}})^{-1}$ as $T_2^{-1} = 24.4 \text{ ms}^{-1} = (41.1 \mu\text{s})^{-1}$ obtained for the $m_s = 0 \leftrightarrow 1$ transition at 49.8 mT driven at 4.2658 GHz [Δ in Fig. 3(c)]. This spin state shares the same decoherence mechanism with the $m_s = 0 \leftrightarrow -1$ one, except for the ID due to the P1 spins. The main contributor to $(T_2^{\text{base}})^{-1}$ is the ID among the NV spins, which, for $N_{\text{NV}||B_0} = 0.25 \times 10^{17} \text{ cm}^{-3}$ (1/4 of the total NV density¹⁵), is estimated to be 20.1 ms^{-1} . The rest (4.3 ms^{-1}) should come from (i) the spectral diffusion caused by flip-flops among the P1 spins and (ii) the T_1 relaxation. The lattice ^{13}C nuclei play a negligible role owing to the isotope enrichment of ^{12}C in this sample.

We then calculate the P1-induced T_{id}^{-1} after subtracting $(T_2^{\text{base}})^{-1}$ from the measured T_2^{-1} and the corresponding P1 densities, which are listed in Table I. In Eq. (3), $\beta = \pi/\sqrt{2}$ is used, due to the smaller rotation angle for the $S = \frac{1}{2}$ P1 spins relative to the $S = 1$ NV spins.³¹ The ratio $(N_{\text{II}} + N_{\text{IV}})/(N_{\text{I}} + N_{\text{V}}) = 3.1$ is close to 3: the ratio of the numbers of P1 centers tilted from and aligned with B_0 . On the other hand, $(N_{\text{I}} + N_{\text{II}} + N_{\text{IV}} + N_{\text{V}})/2 = 0.85 \times 10^{17} \text{ cm}^{-3}$ is less than $N_{\text{III}} = 1.05 \times 10^{17} \text{ cm}^{-3}$. The discrepancy may indicate the presence of an additional $S = \frac{1}{2}$ impurity with the density of $2 \times 10^{16} \text{ cm}^{-3}$. We note that, in samples with the P1 density of $\sim 10^{17} \text{ cm}^{-3}$, the P1-induced spectral diffusion of the order of a few 100 μ s has been observed,^{32,33} consistent with our assignment of a few ms^{-1} decoherence rate to this mechanism.

From the total P1 + NV density of $3.75 \times 10^{17} \text{ cm}^{-3}$, the dipolar-limited linewidth is estimated to be 95 kHz from the second moment.^{34,35} This suggests that the present NV linewidth (250 kHz) is still not limited by the dipolar interactions and there is a room for further reducing the NV linewidth while keeping the NV density at 10^{17} cm^{-3} .

Finally, we examine the T_π -dependence of T_2 , taking Peak IV as an example. T_π of ~ 45 ns used in Fig. 3(c) is so broadband that the linewidth deduced from the multi-Lorentzian fit (16 MHz) does not necessarily reflect the true width. Figure 4(a) demonstrates that, as making T_π longer,

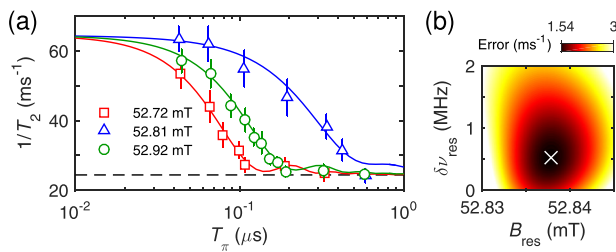


FIG. 4. (a) T_π -dependence of T_2^{-1} at Peak IV. (b) Fit error as a function of fitting parameters B_{res} and $\delta\nu_{\text{res}}$. The cross mark (x) indicates the values giving the best fit.

T_2^{-1} gradually falls down to $(T_2^{\text{base}})^{-1}$, suggesting that less and less P1 spins are flipped. Considering that an *effective* amount of spins rotated is determined from an overlap between the frequency spectrum of the microwave pulse $\mathcal{P} = (f_R/f_{R,g})^2$ and the impurity spin spectrum \mathcal{S} , we write T_π -dependent T_2 as

$$\frac{1}{T_2} = \frac{1}{T_2^{\text{base}}} + D N_{\text{IV}} \int \mathcal{P} \mathcal{S} \sin^2\left(\frac{\beta}{2}\right) df. \quad (4)$$

Here, $f_R = (2\sqrt{2}T_\pi)^{-1}$ is the Rabi frequency for $S=\frac{1}{2}$, $f_{R,g}(f) = \{(f - \delta f)^2 + f_R^2\}^{1/2}$ with $\delta f = 2g\mu_B(B_0 - B_{\text{res}})$ is the generalized Rabi frequency,³⁴ $\beta(f) = 2\pi f_{R,g} T_\pi$ is the flip angle, and $\mathcal{S}(f) = \delta\nu_{\text{res}}/2\pi\{(f - \delta f)^2 + (\delta\nu_{\text{res}}/2)^2\}$ is assumed to be a Lorentzian. Despite the complex form, Eq. (4) contains only two fitting parameters (the resonance magnetic field B_{res} and the impurity spin linewidth $\delta\nu_{\text{res}}$) and yet reproduces the experimental data at $(B_{\text{res}}, \delta\nu_{\text{res}}) = (52.838 \text{ mT}, 520 \text{ kHz})$ [solid lines in Fig. 4(a)]. The extracted P1 linewidth of 520 kHz is broader than the NV linewidth and the dipolar-limited linewidth, hinting at the presence of additional broadening mechanisms in this sample. On the other hand, Fig. 4(b) suggests that, while the error at the best fit is 1.54 ms $^{-1}$, the 200-kHz linewidth can be obtained with the error of 1.68 ms $^{-1}$. Such a small difference in errors can arise, for instance, from the uncertainty in T_1 , which is also B_0 -dependent around the SSR due to cross relaxation.^{36–39} For a more refined estimation of the P1 linewidth, fine-tuning of B_0 to the exact P1 resonance and a detailed measurement of T_1 will be helpful. Nonetheless, the method presented here will be a powerful approach to resolve a spin spectrum when applied to external spins.

In summary, by applying both DNP and pulsed ODMR techniques to a near-surface, narrow-resonance-linewidth NV ensemble, we have shown that a photon-shot-noise-limited magnetic sensitivity of 35 nT Hz $^{-0.5}$, highly promising for 2D magnetic imaging, is attainable. We have also measured T_2 and deduced quantitative information on residual paramagnetic impurities in the sample. Decoherence spectroscopy as demonstrated here is applicable to detect magnetic signals external to the sample. Although the present work focused on the internal P1 spins for the purpose of demonstrating the power of decoherence spectroscopy, the magnetic field can be readily tuned to avoid the P1 resonances while still maintaining DNP. Such a condition is suitable to concurrently perform highly sensitive DC magnetic imaging and decoherence spectroscopy of external spins (supplementary material).

See supplementary material for the feasibility of decoherence spectroscopy in detecting external spins.

W.D.L. acknowledges the support from the NSF of China under Grant No. 61306123 and RGC of HKSAR under Grant No. 27205515. H.W. acknowledges the support from JSPS Grant-in-Aid for Scientific Research (KAKENHI) (A) No. 26249108 and JST Development of Systems and Technologies for Advanced Measurement and Analysis (SENTAN). K.-M.C.F. acknowledges the support from the National Science Foundation under Grant No. 1607869 and RCSA's Cottrell Scholar program. K.M.I. acknowledges support from KAKENHI (S) (No. 26220602), JSPS Core-to-Core Program, and Spintronics Research Network of Japan (Spin-RNJ).

- ¹P. Glover and P. Mansfield, *Rep. Prog. Phys.* **65**, 1489 (2002).
- ²*Magnetic Microscopy of Nanostructures*, edited by H. Hopster and H. P. Oepen (Springer, Berlin, 2005).
- ³R. Schirhagl, K. Chang, M. Loretz, and C. L. Degen, *Annu. Rev. Phys. Chem.* **65**, 83 (2014).
- ⁴B. J. Maertz, A. P. Wijnheijmer, G. D. Fuchs, M. E. Nowakowski, and D. D. Awschalom, *Appl. Phys. Lett.* **96**, 092504 (2010).
- ⁵S. Steinert, F. Dolde, P. Neumann, A. Arid, B. Naydenov, G. Balasubramanian, F. Jelezko, and J. Wrachtrup, *Rev. Sci. Instrum.* **81**, 043705 (2010).
- ⁶L. M. Pham, D. Le Sage, P. L. Stanwix, T. K. Yeung, D. Glenn, A. Trifonov, P. Cappellaro, P. R. Hemmer, M. D. Lukin, H. Park, A. Yacoby, and R. L. Walsworth, *New J. Phys.* **13**, 045021 (2011).
- ⁷D. Le Sage, K. Arai, D. R. Glenn, S. J. DeVince, L. M. Pham, L. Rahm-Lee, M. D. Lukin, A. Yacoby, A. Komeili, and R. L. Walsworth, *Nature* **496**, 486 (2013).
- ⁸D. R. Glenn, K. Lee, H. Park, R. Weissleder, A. Yacoby, M. D. Lukin, H. Lee, R. L. Walsworth, and C. B. Connolly, *Nat. Methods* **12**, 736 (2015).
- ⁹M. Chipaux, A. Tallaire, J. Achard, S. Pezzagna, J. Meijer, V. Jacques, J.-F. Roch, and T. Debuisschert, *Eur. Phys. J. D* **69**, 166 (2015).
- ¹⁰D. A. Simpson, J.-P. Tetienne, J. M. McCoe, K. Ganesan, L. T. Hall, S. Petrou, R. E. Scholten, and L. C. L. Hollenberg, *Sci. Rep.* **6**, 22797 (2016).
- ¹¹J. M. Taylor, P. Cappellaro, L. Childress, L. Jiang, D. Budker, P. R. Hemmer, A. Yacoby, R. Walsworth, and M. D. Lukin, *Nat. Phys.* **4**, 810 (2008).
- ¹²L. Rondin, J.-P. Tetienne, T. Hingant, J.-F. Roch, P. Maletinsky, and V. Jacques, *Rep. Prog. Phys.* **77**, 056503 (2014).
- ¹³J. Wrachtrup, F. Jelezko, B. Grotz, and L. McGuinness, *MRS Bull.* **38**, 149 (2013).
- ¹⁴K. Ohashi, T. Rosskopf, H. Watanabe, M. Loretz, Y. Tao, R. Hauert, S. Tomizawa, T. Ishikawa, J. Ishii-Hayase, S. Shikata, C. L. Degen, and K. M. Itoh, *Nano Lett.* **13**, 4733 (2013).
- ¹⁵E. E. Kleinsasser, M. M. Stanfield, J. K. Q. Banks, Z. Zhu, W.-D. Li, V. M. Acosta, H. Watanabe, K. M. Itoh, and K.-M. C. Fu, *Appl. Phys. Lett.* **108**, 202401 (2016).
- ¹⁶K. M. Itoh and H. Watanabe, *MRS Commun.* **4**, 143 (2014).
- ¹⁷B. Grotz, J. Beck, P. Neumann, B. Naydenov, R. Reuter, F. Reinhard, F. Jelezko, J. Wrachtrup, D. Schweinfurth, B. Sarkar, and P. Hemmer, *New J. Phys.* **13**, 055004 (2011).
- ¹⁸G. de Lange, T. van der Sar, M. Blok, Z.-H. Wang, V. Dobrovitski, and R. Hanson, *Sci. Rep.* **2**, 382 (2012).
- ¹⁹H. J. Mamin, M. H. Sherwood, and D. Rugar, *Phys. Rev. B* **86**, 195422 (2012).
- ²⁰L. P. McGuinness, L. T. Hall, A. Stacey, D. A. Simpson, C. D. Hill, J. H. Cole, K. Ganesan, B. C. Gibson, S. Prawer, P. Mulvaney, F. Jelezko, J. Wrachtrup, R. E. Scholten, and L. C. L. Hollenberg, *New J. Phys.* **15**, 073042 (2013).
- ²¹M. S. Grinolds, M. Warner, K. De Greve, Y. Dovzhenko, L. Thiel, R. L. Walsworth, S. Hong, P. Maletinsky, and A. Yacoby, *Nat. Nanotechnol.* **9**, 279 (2014).
- ²²L. Luan, M. S. Grinolds, S. Hong, P. Maletinsky, R. L. Walsworth, and A. Yacoby, *Sci. Rep.* **5**, 8119 (2015).
- ²³D. Schmid-Lorch, T. Häberle, F. Reinhard, A. Zappe, M. Slota, L. Bogani, A. Finkler, and J. Wrachtrup, *Nano Lett.* **15**, 4942 (2015).

- ²⁴A. Dréau, M. Lesik, L. Rondin, P. Spinicelli, O. Arcizet, J.-F. Roch, and V. Jacques, *Phys. Rev. B* **84**, 195204 (2011).
- ²⁵V. Jacques, P. Neumann, J. Beck, M. Markham, D. Twitchen, J. Meijer, F. Kaiser, G. Balasubramanian, F. Jelezko, and J. Wrachtrup, *Phys. Rev. Lett.* **102**, 057403 (2009).
- ²⁶R. Fischer, A. Jarmola, P. Kehayias, and D. Budker, *Phys. Rev. B* **87**, 125207 (2013).
- ²⁷T. Wolf, P. Neumann, K. Nakamura, H. Sumiya, T. Ohshima, J. Isoya, and J. Wrachtrup, *Phys. Rev. X* **5**, 041001 (2015).
- ²⁸W. V. Smith, P. P. Sorokin, I. L. Gelles, and G. J. Lasher, *Phys. Rev.* **115**, 1546 (1959).
- ²⁹R. Hanson, O. Gywat, and D. D. Awschalom, *Phys. Rev. B* **74**, 161203 (2006).
- ³⁰J. R. Klauder and P. W. Anderson, *Phys. Rev.* **125**, 912 (1962).
- ³¹A. Schweiger and G. Jeschke, *Principles of Pulse Electron Paramagnetic Resonance* (Oxford University Press, Oxford, 2001).
- ³²L. M. Pham, N. Bar-Gill, C. Belthangady, D. L. Sage, P. Cappellaro, M. D. Lukin, A. Yacoby, and R. L. Walsworth, *Phys. Rev. B* **86**, 045214 (2012).
- ³³N. Bar-Gill, L. M. Pham, A. Jarmola, D. Budker, and R. L. Walsworth, *Nat. Commun.* **4**, 1743 (2013).
- ³⁴A. Abragam, *Principles of Nuclear Magnetism* (Oxford University Press, Oxford, 1961).
- ³⁵J. A. van Wyk, E. C. Reynhardt, G. L. High, and I. Kiflawi, *J. Phys. D: Appl. Phys.* **30**, 1790 (1997).
- ³⁶A. Jarmola, V. M. Acosta, K. Jensen, S. Chemerisov, and D. Budker, *Phys. Rev. Lett.* **108**, 197601 (2012).
- ³⁷M. Mrózek, D. Rudnicki, P. Kehayias, A. Jarmola, D. Budker, and W. Gawlik, *EPJ Quantum Technol.* **2**, 22 (2015).
- ³⁸L. Hall, P. Kehayias, D. A. Simpson, A. Jarmola, A. Stacey, D. Budker, and L. C. L. Hollenberg, *Nat. Commun.* **7**, 10211 (2015).
- ³⁹J. D. A. Wood, D. A. Broadway, L. T. Hall, A. Stacey, D. A. Simpson, J.-P. Tetienne, and L. C. L. Hollenberg, *Phys. Rev. B* **94**, 155402 (2016).